

Isotopic and hydrochemical evidence of groundwater recharge in the Hopq Desert, NW China

Jian Ge¹ · Jiansheng Chen^{1,2} · Lu Ge² · Tao Wang¹ · Chao Wang² · Yafei Chen¹

Received: 8 February 2016 / Published online: 3 May 2016
© Akadémiai Kiadó, Budapest, Hungary 2016

Abstract Artesian wells and lakes are found in the hinterland of the Hopq Desert, China. Analysis of soil profiles has revealed that the local vadose zone is always in a state of water deficit because of strong evaporation, and precipitation cannot infiltrate into the groundwater. This research indicated that soil water and surface water are recharged by groundwater and that the groundwater is recharged via an external source. Analyses of the stable isotopes in precipitation and of the water budget suggested that surface water in the Qiangtang Basin on the Tibetan Plateau might correspond to the groundwater in the Hopq Desert.

Keywords Isotopic tracers of deuterium and oxygen 18 · Hydrochemical signatures · Soil profiles · Hopq Desert · Hydrological cycle

Introduction

The Hopq Desert is an arid region in the northern part of the Ordos Basin, where precipitation (evaporation) decreases (increases) from the southeast to the northwest. Although the climate is arid and precipitation is scant, groundwater is abundant. The Chinese Geological Survey

found that the annual average recharge of groundwater in the Ordos Basin is about $1.05 \times 10^{11} \text{ m}^3$ [1]. Furthermore, compared with southern parts, groundwater in the Hopq Desert is more abundant and of better quality, and the water reserved in deep aquifers are greater than in shallow aquifers. This abnormal phenomenon has aroused wide concern and academic interest in the hydrological field [2–6].

According to the theory of regional hydrological circulation, some researchers hold the opinion that groundwater in the Hopq Desert is recharged by local precipitation. The regional aeolian sand is permeable to infiltration by rainwater, which is cited as an explanation for the greater abundance and better quality of the groundwater in the northern desert than in southern parts of the region [4, 5]. However, simulated precipitation tests in Wuhai, on the western margin of the Hopq Desert, have shown that the maximum depth of penetration from 150 mm of rainfall would be <1000 mm [7]. Another simulation test has shown that 59 mm of rainfall would only penetrate about 460 mm into the sand [7]. Based on such experiments, it has been proposed that although the aeolian sand is highly conductive to water, rainwater alone could not account for the recharge of groundwater when the moisture content of the soil is far below the maximum field capacity.

In order to prove that groundwater is recharged by precipitation, the inverse geochemical modelling method [8, 9] and the groundwater dating method, based on the $^{14}\text{C}/^{12}\text{C}$ ratio, have been applied [10, 11]. However, previous research on rock inclusions has proven that the dolomitization temperature in the Hopq Desert was 104–368 °C, not the ordinary temperature [12, 13], and that the ^{13}C enrichment in the Hopq dolomite indicated that precipitation did not participate in the process of dolomitization [14]. Furthermore, because carbonaceous gases

✉ Jiansheng Chen
jschen@hhu.edu.cn

¹ College of Civil and Transportation Engineering, Hohai University, No. 1 Xikang Road, Nanjing 210098, Jiangsu Province, China

² School of Earth Science and Engineering, Hohai University, No. 1 Xikang Road, Nanjing 210098, Jiangsu Province, China

such as CO_2 , CO , and CH_4 from deep strata dissolved into the groundwater, the results of $^{14}\text{C}/^{12}\text{C}$ ratio dating were negatively affected by the ^{12}C (dead carbon) from other sources. The mixed dead carbon makes the age of the deep groundwater appear older than its actual age [15]. Therefore, the above examples claiming that groundwater in the Hopq Desert is recharged by local precipitation could be questionable.

Contrary to the theory that groundwater in the Hopq Desert is recharged by local precipitation, an opposing academic viewpoint is that the groundwater originates from an external source. Given the facts that the underground watersheds in the Hopq Desert do not correspond with precipitation but with bedrock fault zones instead, and that the precipitation and groundwater isotopic signatures are obviously different, it can be implied that the groundwater could be derived largely from outside the region [16, 17]. The vadose zone is the first chain in precipitation infiltration. Therefore, analyses of soil profiles could be used to estimate the transport and migration of isotopic tracers such as deuterium and oxygen 18, moisture, and some solvents, and comparison with data from surface water, groundwater, and precipitation could reflect the relative importance of the recharge and discharge by the different sources of water. However, little relevant research has been conducted and thus, the full characteristics of the hydrological circulation of the Hopq Desert remain uncertain.

Analyses of stable isotopic tracers, hydrochemical signatures, and soil profiles can be applied to trace and probe the evolution of different sources of water. Such methods have been proven practical and inexpensive tools in hydrology research, especially in arid and semiarid areas, and are incomparable to other techniques [18–25]. For example, by measuring the stable isotope values and hydrochemical concentrations, Dogramaci et al. [26] studied groundwater evolution in a sub-tropical semiarid basin in Australia. Song et al. [27] investigated the stable isotopes of deuterium and oxygen 18 in soil water, groundwater, and precipitation to reveal that heavy and long-lasting rainfall events were the main recharge source in the Mt. Taihang area of northern China. The mean residential times of shallow groundwater were also estimated. At the Mt. Vulture volcano, southern Italy, variations of the stable isotopes of rainwater and groundwater and the local vertical isotopic gradient of $\delta^{18}\text{O}$, have been used to explore the weighted local meteoric water line. Some anomalous isotopic signatures were used to explain the ascent of deeper groundwater [28].

The Hopq Desert, which is a region that is extremely arid but with abundant groundwater, was chosen as the study area for this research, where soil profile, stable isotopic, and hydrochemical analyses were performed. Samples from surface water (rivers, lakes, and water

reservoirs), groundwater (shallow wells, deep wells, artesian wells, and hot springs), and pore water extracted from soil profiles (SPs) were collected and analyzed for their compositions of deuterium, oxygen 18, K^+ , Na^+ , Ca^{2+} , Mg^{2+} , CO_3^- , HCO_3^- , SO_4^{2-} , and Cl^- . This study had two principal objectives: (1) to decipher the hydrological relationships between the precipitation, surface water, soil water, and groundwater in the Hopq Desert region; and (2) to explore the origin of the local groundwater and its circulation regularity.

Study area

The Hopq Desert (Fig. 1) is located in the northern part of the Ordos Sedimentary Basin ($39^\circ 59.2' - 40^\circ 49.3'\text{N}$, $106^\circ 52.6' - 111^\circ 19.2'\text{E}$). It extends for approximately 400 km from east to west and 20–80 km from south to north, encompassing an area of about 15,000 km^2 . It is bordered by the Yellow River to the west, north, and east, and the Mu Us Sand Land to the south. It has a temperate arid plateau continental climate, with mean annual precipitation reducing from 300 mm in the southeast to 150 mm in the northwest. Influenced by the southeast monsoon, about 60–80 % of the annual rainfall occurs from July to September (only 3–5 % occurs in winter). The potential evaporation is 2000–3000 mm/a. The annual average temperature is 6.0–8.5 $^\circ\text{C}$, and the average temperature in January and July is -11.8 and 22.1 $^\circ\text{C}$, respectively. The maximum wind velocity is 30.0 m/s and there are on average 28 days on which the maximum wind velocity exceeds 17.2 m/s [29, 30].

The elevation of the Hopq Desert ranges from 1257 to 1050 m a.s.l. and the topography rises slowly from the northeast to the southwest. From south to north, there are three main types of landscape: tectonic tableland, aeolian sand dunes, and the Yellow River alluvial land. The rock strata, from the base upward, comprise Precambrian metamorphic bedrock, Jurassic siltstone and mudstone, Cretaceous sandstone, Paleogene and Neogene mudstone and sandstone, and Quaternary sediment [3, 5, 16]. Based on a hydrogeological investigation from 1999 to 2006, the major water-bearing formations in the Hopq Desert were established as the Cretaceous carbonate aquifer system and the Quaternary aquifer system. The Cretaceous carbonate aquifer system, which is the dominant water-bearing formation with a thickness of up to 1200 m, can be subdivided from bottom to top into three sub-formations: the Luohe Formation, Huanhe Formation, and Luohandong Formation. The annual average recharge of groundwater in the Cretaceous carbonate aquifer system is estimated to be $6.72 \times 10^9 \text{ m}^3$ [31]. Different sizes of bedrock faults have been found in the north of the Ordos Basin, which

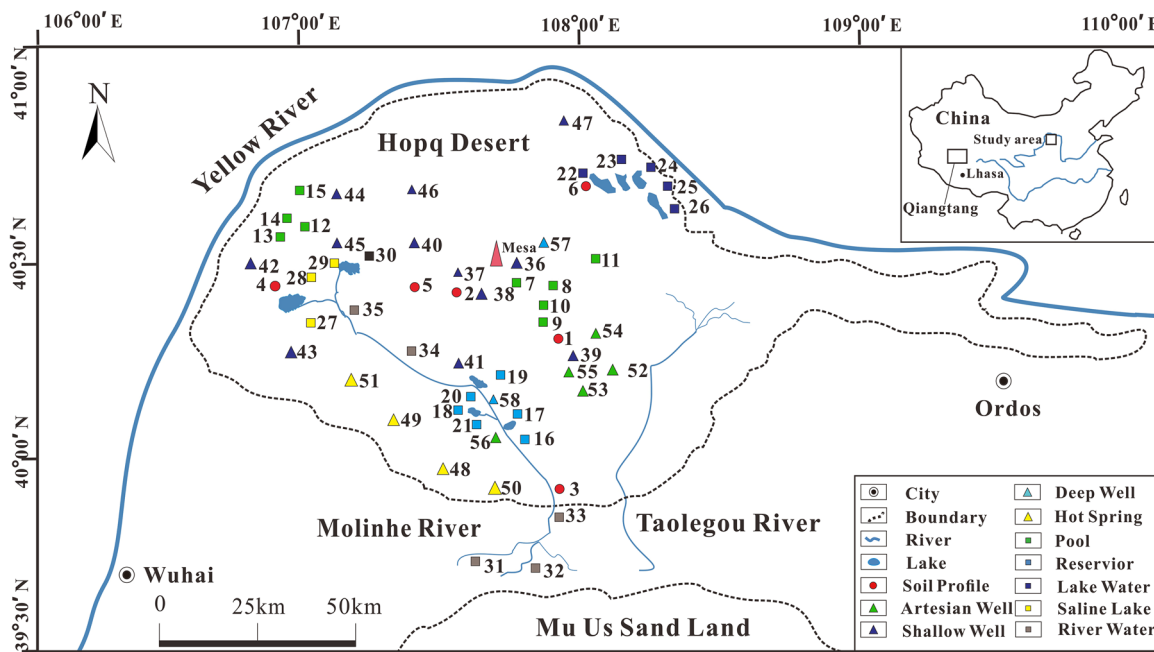


Fig. 1 Map of study area showing the sampling locations

obviously have regional distribution. The southeast and northwest regions of the Hopq Desert are dominated by NE-trending and NW-trending fault zones, respectively [32, 33].

Although the local climate is extremely dry, there are several artesian wells (Fig. 2a, b) scattered within the central region of the desert. The ground elevations of the artesian wells range from 1165 to 1197 m a.s.l. The artesian flow is relatively stable and it is not influenced by variation of precipitation, which implies that the artesian wells are recharged by a constant water source. Lakes and ponds are found in the desert hinterland (Fig. 2c, d). The ground elevations of the lakes range from 1049 to 1193 m a.s.l. The areas of the lakes demonstrate periodic regulation, i.e., expanding in spring and contracting in summer. Inland rivers such as the Molin and Taolegou rivers show the same variation tendency that is unaffected by the season. The local rainy season persists from July to September, but the flood period of the local rivers appears in late spring, which implies they could have a recharge source other than rainwater.

Sampling and methods

Sampling

The field investigation and sample collection in the Hopq Desert were conducted from October 13–24, 2014. The sampling locations are shown in Fig. 1. Overall, 23

groundwater samples comprising 12 shallow wells (depth <20 m), 5 artesian wells, 2 deep wells (depth approx. 150 m), and 4 hot-springs; and 29 surface water samples comprising 9 ponds, 6 reservoirs, 5 lakes, 4 salt lakes, and 5 rivers, were collected from the hinterland and surrounding areas of the Hopq Desert. The samples were stored in 550-ml polyvinyl chloride bottles that were sealed tightly with adhesive tape to avoid undesired isotopic fractionation.

Excavation of the soil samples was conducted at the same time as the water sample collection. The maximum profile depth was 7.2 m and the minimum was 2.4 m. Sand samples were collected at 20-cm intervals, which generated 129 soil samples in total. Details concerning the locations of the soil profiles and their features are presented in Table 1. The site of each soil profile was selected such that the effects of anthropogenic influences could be neglected. SP1 is located in the artesian region with a groundwater level (GL) of –60 cm. SP2 (Fig. 2e) is on the southern slope of a volcanic mesa with an elevation of 1235 m a.s.l. and a GL of –2.90 m. The positions of SP3 and SP4 are on the upper and lower reaches of the Molin River. SP5 (Fig. 2f) is between two sand dunes where the depth of plant roots is about 1.5 m. SP6 is on the northern margin of the study area and near the Qixing Lake. The first 1.0 m of the soil profile was sampled in an open pit in case of borehole collapse as the deeper parts were sampled using a sand-sampling auger. The 350-g samples of soil collected in the field were sealed in airtight bags.

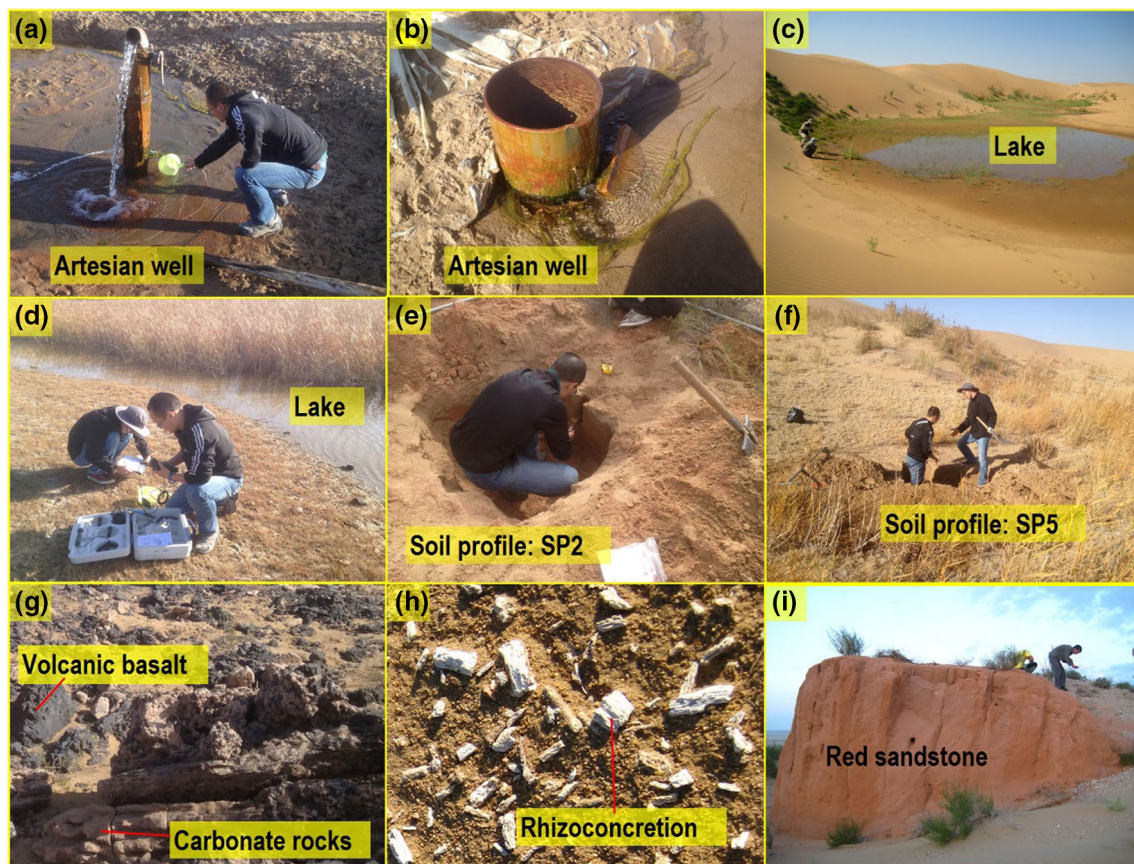


Fig. 2 Artesian wells, lakes, volcanic basalt, rhizoconcretion, red sandstone stratum, and some examples of fields of soil profile excavation in the Hopq Desert. **a** and **b** two artesian wells in the central part of the study area; **c** and **d** two lakes and the surrounding

areas; **e** and **f** two locations of excavation of soil profiles (the first 1 m of the profile was sampled in an open pit in case of collapse); **g** basalt and carbonate rocks found on the tops of some monticules; **h** debris of rhizoconcretions; and **i** outcropping of red sandstone stratum

Table 1 Locations and descriptions of the features of the six soil profiles

Profile ^a	Longitude (E)	Latitude (N)	Elevation (m)	Depth (cm)	GL (cm)	Features description
SP1	108°9.3'	40°23.3'	1167	240	−60	Artesian area, vegetation flourish, aeolian sand
SP2	107°55.1'	40°27.7'	1235	320	−290	Southern face of a mesa, plants flourish, −2~−3 m red clay layer found
SP3	107°53.5'	39°59.2'	1182	700	−690	Upper reach of Molin River, medium plants, −3 m red clay particles found
SP4	107°30.7'	40°28.8'	1049	320	−	Lower reach of Molin River, salinization, −2 m red clay particles found
SP5	107°50.0'	40°28.3'	1161	500	−220	Lower land between two sand dunes, plants flourish, aeolian sand
SP6	108°19.4'	40°39.5'	1035	500	−490	Qixing Lake area, no plants, −1~−2 m red clay particles found

^a SP1–SP6 represent sampling points 1–6 on Fig. 1

Methods

Prior to the laboratory analyses, samples were subjected to a series of pre-treatment processes. Vacuum distillation and a cold trap set were used to collect soil water for the

stable isotopic analysis [34, 35]. Soil samples for the chemical analyses were pre-treated as follows. First, the soil sample was baked in a drying oven at 105 °C for 24 h. Then, 20 g of the baked soil sample was mixed with 100 ml of deionized water and blended periodically for

48 h. Finally, the mixed liquid was filtered using a 0.25- μm Millipore medium-speed screen to obtain the supernatant solution suitable for the chemical analysis [36]. The value of the total dissolved solids (TDS) of the soil samples could be converted from the TDS value of their supernatant solutions.

In the field, general parameters such as the temperature, potential of Hydrogen (pH), TDS, electrical conductance (EC), and salinity of the samples were measured using a portable multifunction field meter (Multi3400i series, WTW GmbH, Munich, Bavaria, Germany), which has an error of measurement of $<10\%$. In the laboratory, the δD and $\delta^{18}\text{O}$ values were analyzed using a mass spectrometer (MAT 253, Thermo Fisher-Finnigan, Waltham, Massachusetts, USA), which has a deviation of ≤ 0.1 and $\leq 2\%$ for the oxygen and hydrogen isotopes, respectively. The CO_2 and H_2 gases produced using the $\text{CO}_2\text{-H}_2\text{O}$ equilibration method [37] and the zinc reduction method [38] were used for the analyses of the oxygen and hydrogen isotopes, respectively. The values of deuterium and oxygen 18 were calibrated against reference materials and standards from the International Atomic Energy Agency [39, 40], and they were reported in the form of per mil (‰) with the notation of δ . Measurements of positive ions such as Ca^{2+} , Mg^{2+} , Na^+ , and K^+ were obtained using an ICP-OES Spectrometer (iCAP 6000 Series, Thermo Fisher, Waltham, Massachusetts, USA); measurements of negative ions such as SO_4^{2-} , Cl^- , and NO_3^- were obtained using an ion chromatography instrument (ICS-2000 series, Dionex, Sunnyvale, California, USA). The precision for the cation and anion measurements was $>95\%$. Other anions such as CO_3^{2-} and HCO_3^- were analyzed using phenolphthalein and methyl-orange double indicator titration. The samples were analyzed at the State Key Laboratory of Hydrology-Water Resources and Hydraulic Engineering of Hohai University, China.

The landscape of the Hopq Desert is relatively plain without any mountains of significance that could obstruct rain clouds and thus, the stable isotopes of local precipitation should have the same characteristics as the surrounding areas. Referring to data from the Global Network of Isotopes in Precipitation (GNIP) and previous references, the monthly isotopic averages of δD and $\delta^{18}\text{O}$ in precipitation are shown in Fig. 3, together with the monthly averages of total rainfall in the Ordos Basin [41]. It can be seen that while δD and $\delta^{18}\text{O}$ in the precipitation are depleted from November to the following February, they are enriched from April to August. In winter, the Hopq Desert is influenced by cold and dry air masses that originate from the Arctic area, which become mixed with continental evaporation such that winter rainwater is depleted in deuterium and oxygen 18. From April to August, rainfall events are dominated mainly by the East

Asian monsoon, which transfers warm and moist air from the Pacific Ocean; hence, the rainwater is enriched in deuterium and oxygen 18. Because of these precipitation effects, the maxima of deuterium and oxygen 18 appear from April to May, while the minima appear in December to the following January [41, 42].

Results

Stable isotopes of hydrogen and oxygen in groundwater and surface water

The values of δD and $\delta^{18}\text{O}$ distributions in the precipitation, surface water, and groundwater of the Hopq Desert are shown in Fig. 4. The weighted averages of δD and $\delta^{18}\text{O}$ of the monthly precipitation are -51.43 and -7.64% , respectively, which are near the values of δD and $\delta^{18}\text{O}$ of precipitation in July and August. Assuming that local surface water and groundwater originate from the meteoric water, the relevant values of δD and $\delta^{18}\text{O}$ should plot along evaporation line 2 (Fig. 4; EL2), the fitted line of local precipitation. However, instead, the points of δD and $\delta^{18}\text{O}$ reflecting the surface water and groundwater plot along evaporation line 1 (Fig. 4; EL1), the fitted line of groundwater, soil water, and surface water in the Hopq Desert. This means that the surface water and groundwater might not be supplied from local precipitation.

The δD and $\delta^{18}\text{O}$ values of surface water are plotted in the upper-right portion of line EL1 and the values of groundwater are plotted in the lower-left portion of EL1 (Fig. 4), meaning that the surface water is recharged mainly from groundwater. The points of groundwater, artesian wells, and springs are plotted lower on the line than shallow wells, which implies that the shallow wells experience relatively strong evaporation. For the same reason, the δD and $\delta^{18}\text{O}$ values of lakes, ponds, and salt lakes plot higher along the line than rivers and reservoirs.

Stable isotopes of hydrogen and oxygen in soil profiles

The δD and $\delta^{18}\text{O}$ profiles of the soil water are shown in Fig. 5. The values of δD and $\delta^{18}\text{O}$ fluctuate significantly from -2.0 m to ground level; usually, the maxima appear at the top of the profile, whereas they tend to be less changeable below -2.0 m. Obviously, the δD and $\delta^{18}\text{O}$ distributions of each soil profile correspond to the intensity of evaporation, which causes δD and $\delta^{18}\text{O}$ to be enriched in the upper portion and relatively depleted exponentially in the middle and lower portions [44, 45]. Below -2.0 m, δD values from SP1–SP5 and $\delta^{18}\text{O}$ values from SP1–SP6 are depleted by more than -51.43 and -7.64% ,

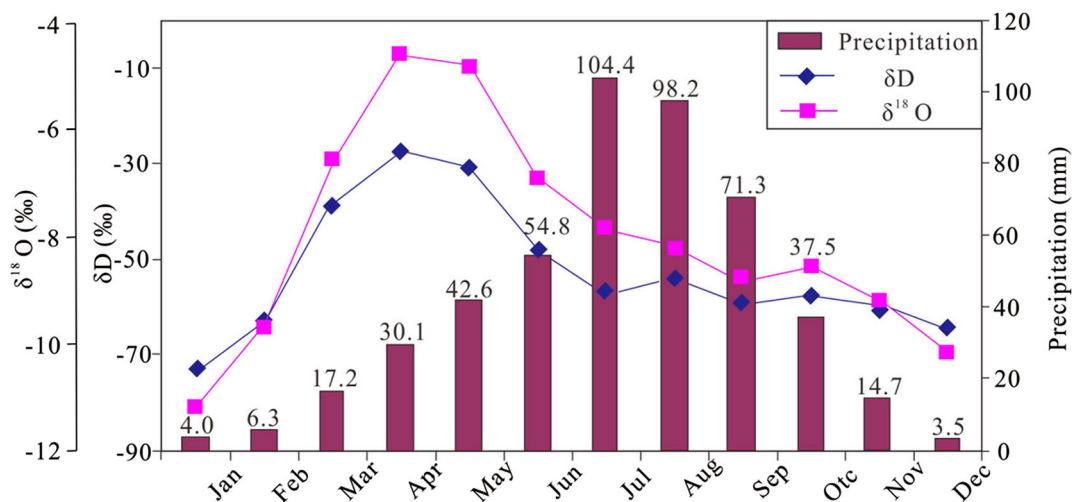


Fig. 3 Monthly isotopic averages of δD versus $\delta^{18}O$ in precipitation and monthly averages of total rainfall in the Ordos Basin [41]. The monthly averages of total rainfall range from 3.52 to 6.25 mm in winter and from 54.40 to 104.37 mm in summer. The monthly weighted averages of δD and $\delta^{18}O$ in precipitation are depleted in

April (-27.68 , -4.63 ‰), and enriched in January (-73.50 , -11.22 ‰) with annual weighted averages of -51.43 and -7.64 ‰, respectively. Among the 270 precipitation samples, 150 samples were from GNIP stations (1985–2000) and the other 120 samples were from the Chinese Geological Survey (1999–2005)

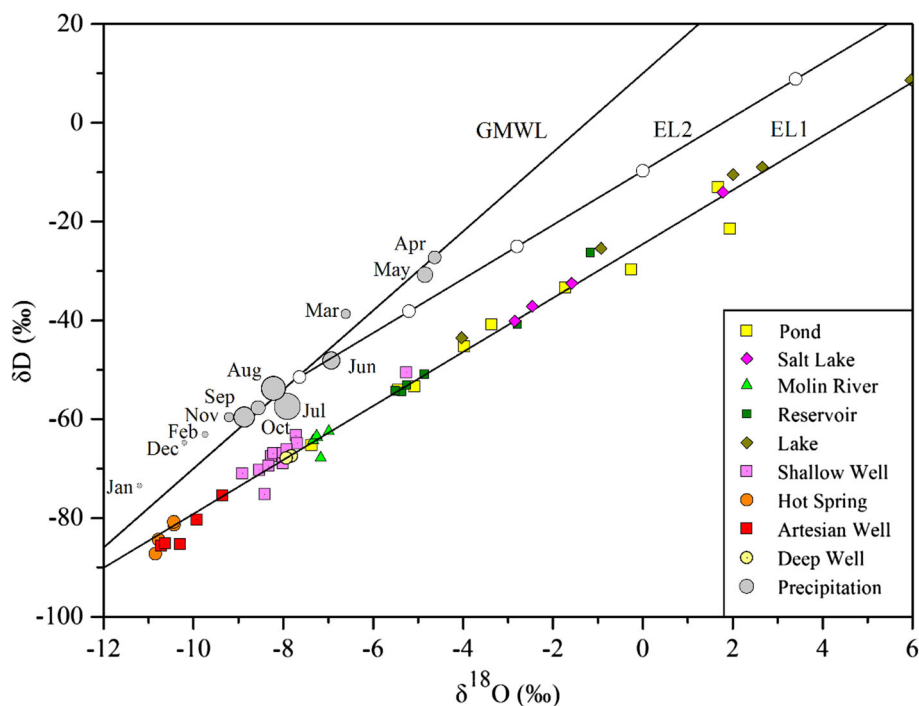


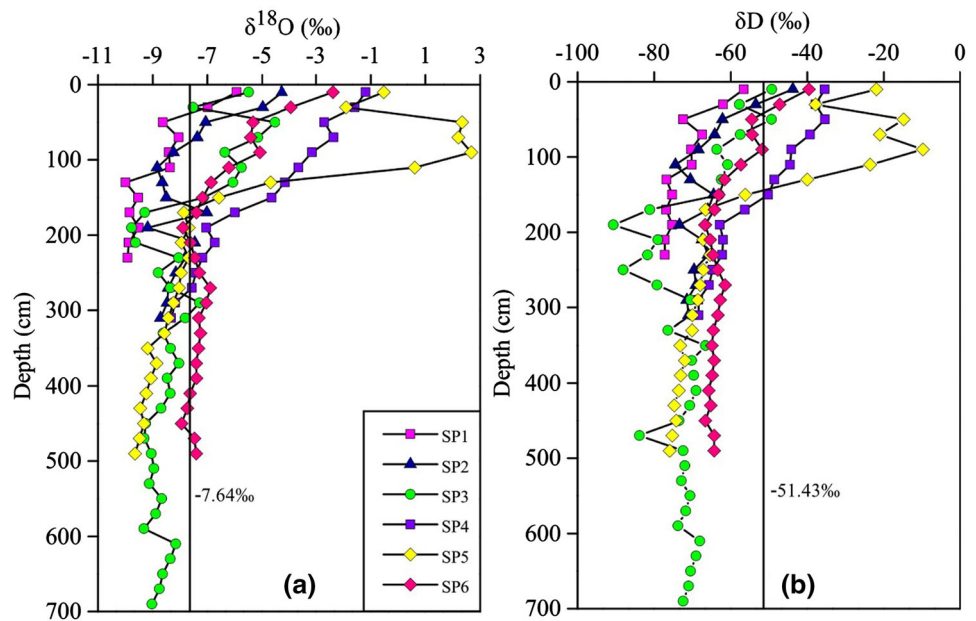
Fig. 4 Isotopic values of δD versus $\delta^{18}O$ for precipitation, surface water, and groundwater in the Hopq Desert. Monthly weighted averages of δD and $\delta^{18}O$ of precipitation are plotted as gray points [41]. The area of each point correlates with the monthly averages of total rainfall. GMWL is the global meteoric water line: $\delta^2H = 8\delta^{18}O + 10$ [43]. EL1 is the evaporation line ($\delta D = 5.4\delta^{18}O - 24.53$, $n = 181$, $r^2 = 0.953$) fitted from the δD and $\delta^{18}O$ values of

groundwater, soil water, and surface water sampled from October 13–24, 2014. As there was no rainfall event during the survey and because of the intense evaporation, the influence of precipitation on the samples could be neglected. EL2, which parallels EL1, is the evaporation line fitted from the δD and $\delta^{18}O$ values of local precipitation. The intersection point of EL2 and GMWL (-7.64 , -51.43 ‰) is the weighted average of local precipitation

respectively, in comparison with the weighted averages of δD and $\delta^{18}O$ in the local precipitation. This is a reliable indicator that rainwater does not recharge the deep sand

layer of the vadose zone or the groundwater. Presuming precipitation could reach below -2.0 m, the relevant δD and $\delta^{18}O$ values of the soil water should become enriched

Fig. 5 Values of δD and $\delta^{18}O$ versus depth in the six soil profiles. **a** Values of δD versus depth and **b** values of $\delta^{18}O$ versus depth. The vertical line in (5-1) is $\delta^{18}O = -7.64 \text{ ‰}$, i.e., the weighted average of $\delta^{18}O$ in the precipitation. It indicates that (apart from SP6) below -2.0 m , the $\delta^{18}O$ values of most soil water samples are more depleted than the precipitation. The vertical line in (5-2) is $\delta D = -51.53 \text{ ‰}$, i.e., the weighted average of δD in precipitation. It indicates that below -2.0 m , the $\delta^{18}O$ values of all soil water samples are more depleted than the precipitation



by more than -51.43 and -7.64 ‰ , respectively, because of Rayleigh fractionation caused by strong evaporation [46]. The maximum amount of a single precipitation event is $<50 \text{ mm}$. From ground level to -2.0 m , the average gravimetric moisture content of the six soil profiles is 2.13 ‰ , and the maximum field water capacity of aeolian sand is 5 ‰ [47, 48]. Therefore, assuming that all the rainwater was input into the soil, the maximum depth of penetration for a 50-mm precipitation event would be 1.74 m .

The values of δD and $\delta^{18}O$ of the soil samples are shown in Fig. 6. For SP 1 and 2, below -0.5 m , the soil water isotopic data overlap with the groundwater data, which is because the groundwater level of SP1 is -0.6 m and the red sandy soil at SP2, at a depth of -0.9 to -1.3 m , has a higher water-holding capacity. For the other soil profiles, the soil water points below -2.0 m plot along line EL1 (Fig. 6) in the groundwater range. Except for one point above line EL2 and two points between lines EL1 and EL2, all other points plot along line EL1 (Fig. 6), which indicates that the vadose zone is recharged mainly from groundwater and that infiltrated precipitation might have a constrained influence in the topsoil.

Moisture content, TDS, and chloride in the soil profiles

The gravimetric moisture content, TDS, and chloride profiles of SP1–SP6 are shown in Fig. 7. The groundwater levels in the Hopq Desert are relatively shallow, varying from -0.6 to -6.9 m . Except for the TDS profile at SP1 (GL = -0.6 m , TDS maximum on the ground), the TDS and chloride peaks of the other soil profiles appear in the

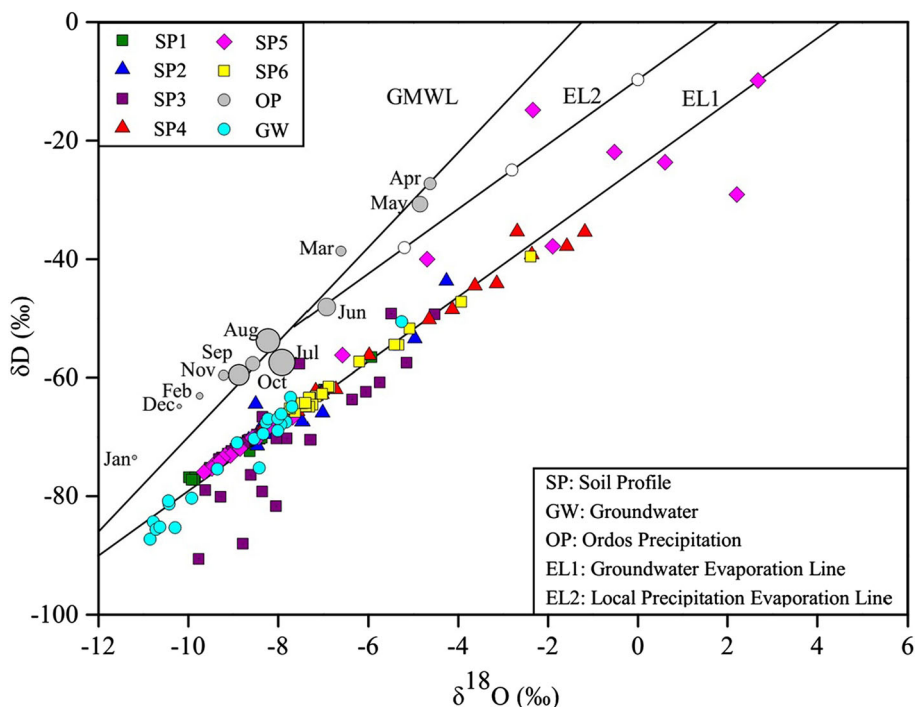
range -0.3 to -4.0 m and generally above the GL. This implies that rainwater does not infiltrate into the groundwater in most parts of the Hopq Desert.

In Fig. 7, SP1 is the only profile in which the moisture content exceeds the maximum field water capacity, which is because it is located within the artesian area. Except for SP1, the other five moisture content profiles indicate a certain degree of water deficit. The water deficit in SP2–SP6 is estimated to be about $44.7\text{--}103.3 \text{ mm}$. During rainfall infiltration, the water deficit in vadose zone should be filled first. The maximum monthly rainfall in the Hopq Desert is 64.2 mm in August [49]. Assuming that the August rainfall infiltrates entirely into the vadose zone without evaporation, the moisture content in SP1 and SP6 could reach the MFWC, whereas the other soil profiles remain in deficit. The value of 64.2 mm of precipitation represents the total amount of rainwater in August. In fact, rainfall events in the Hopq Desert are episodic and sporadic, even in the rainy season and therefore, during intervals between rainfall events, evaporation is intense. It can be determined that the vadose zone in the Hopq Desert is recharged predominantly by groundwater, because the δD and $\delta^{18}O$ values of soil water plot alongside line EL1 (Fig. 6). Therefore, recharge by the upward movement of groundwater represents the constant and important water source required to maintain the sand dunes [50].

Major hydrochemical parameters in groundwater and surface water

The chemical composition of groundwater is affected mainly by the interaction between water and the host

Fig. 6 Values of δD and $\delta^{18}O$ for soil water and precipitation in the Hopq Desert



lithology during underground runoff [51, 52]. The values of TDS in the groundwater in the Hopq Desert are 0.52–2.22 g/L (average: 1.65 g/L). The average TDS values of the artesian, shallow, and deep wells are 1.59, 1.68, and 0.55 g/L, respectively. The TDS values of the Hopq Desert surface water of 1.36–12.7 g/L (average: 3.89 g/L) are obviously higher than the groundwater. The values of TDS in the groundwater and surface water demonstrate that the quality of the groundwater is generally better than the surface water and that the quality of the deep groundwater is the best. Based on the values generated using the AqQA version 1.1 water analytical software [53], four water types can be identified in the study area: Na–Cl, Na–Cl–SO₄, Ca–SO₄–Cl, and Ca–HCO₃. Most of the surface water and shallow groundwater is Na–Cl type; however, water from the deep aquifer is the Ca–HCO₃ type and it is less mineralized.

The Durov diagram [54] of major ions of the groundwater and surface water is shown in Fig. 8. The variations of the major chemical compositions indicate that the ions of Ca²⁺, Na⁺, SO₄²⁻, and Cl⁻ in the deep wells are the lowest and that they become accumulated in the shallow aquifers; the highest concentrations are shown by the surface water. Taking Cl⁻ as an example, the relative concentrations of Cl⁻ in the deep wells are 30–40 %, increasing to 50–60 % in the shallow groundwater, and peaking at up to 60–90 % in the surface water. In contrast, the relative concentrations of HCO₃⁻ in the deep wells are 40–50 %, decreasing to 10–20 % in the shallow wells, and

falling to about 5 % in the surface water. Generally, ions such as Ca²⁺, Na⁺, SO₄²⁻, and Cl⁻ possess high migration ability in water runoff, becoming concentrated along the direction of water flow, whereas HCO₃⁻ and CO₃²⁻ ions have different behaviors [55]. Carbonate ions react with Ca²⁺ or Mg²⁺ in hard water creating carbonate deposition. Moreover, the basicity of the surface water in the Hopq Desert has been enhanced because of the effect of salinization, which makes part of the bicarbonate convert to carbonate, facilitating insoluble carbonates and consuming more HCO₃⁻ and CO₃²⁻ ions. Based on the fact that ions such as Ca²⁺, Na⁺, SO₄²⁻, and Cl⁻ become concentrated and ions such as HCO₃⁻ and CO₃²⁻ become depleted through deep aquifers to the surface water, it could be deduced that in the Hopq Desert deep groundwater recharges shallow groundwater and that it eventually ends up as surface water.

In the process of the upward movement of groundwater, the dissolution of evaporates such as gypsum, sodium sulfate (mirabilite), and halite gradually augments the ionic concentrations of Ca²⁺, Na⁺, SO₄²⁻, and Cl⁻. Furthermore, they condense in the surface water and soil water because of the intense evaporation in the desert. Scatter plots of some of the major chemical ions are shown in Fig. 9. Figure 9a shows the relationships between Na⁺ and Cl⁻ in the groundwater and surface water. The regression line is $y = 1.30x - 2.15$ ($n = 44$, $r^2 = 0.83$), which indicates a positive correlation between Na⁺ and Cl⁻. The dissolution of halite is the main source of Na⁺ and Cl⁻ in

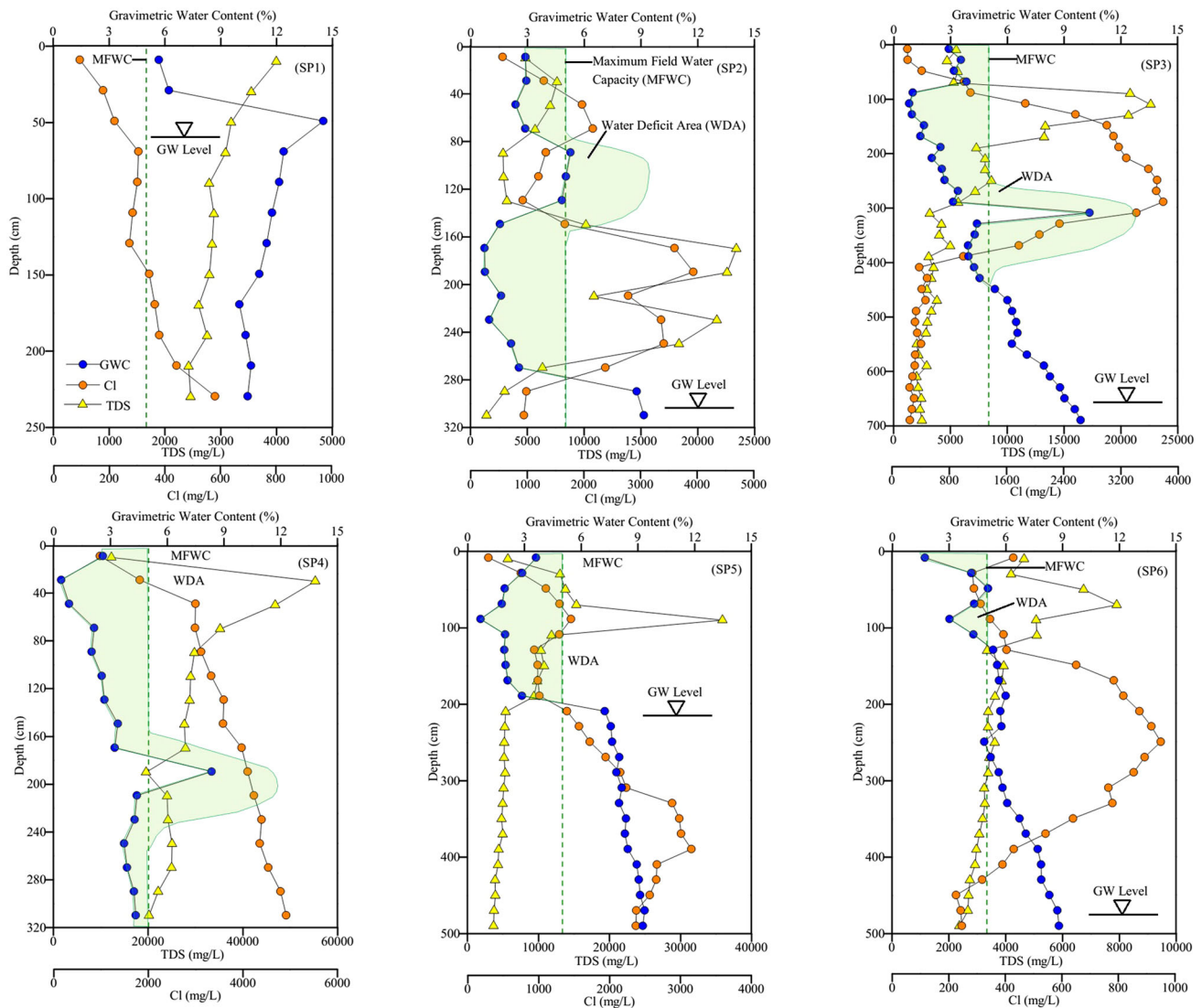


Fig. 7 Values of gravimetric moisture content, TDS, and chloride versus depth. The maximum field water capacity (MFWC) of aeolian sand is 5 % and it changes with the different soil textures within the soil profiles. The groundwater levels for the different soil profiles are

marked (SP4 is the only profile in which groundwater was not discovered). The *light green shading* in SP2–SP6 indicates the soil water deficit areas (WDA), indicating a soil moisture content below the MFWC. (Color figure online)

the groundwater and surface water. Most of the points plot below the line $y = x$, reflecting that Na^+ outweighs Cl^- and that the surplus amount of Na^+ might come from the dissolution of mirabilite in the aeolian sand. Using $(\text{Na}^+ - \text{Cl}^-)$ to represent the extra Na^+ from mirabilite dissolution, the scatter plot of $(\text{Ca}^{2+} + \text{Na}^+ - \text{Cl}^-)$ and SO_4^{2-} is illustrated in Fig. 9b, in which the regression line is $y = 0.87x - 0.48$ ($n = 44, r^2 = 0.76$). It means that mirabilite and gypsum are the main sources of Ca^{2+} , SO_4^{2-} , and part of the Na^+ in the groundwater and surface water of the Hopq Desert. Figure 9b shows that the sum of the anions outweighs the sum of the cations. It implies that except for the dissolution of mirabilite and gypsum, the extra SO_4^{2-} might be derived

from the oxidation of pyrite [56] or the SO_2 gas in coal combustion [57]. The relationship between Na^+ and HCO_3^- is plotted in Fig. 9c, which indicates that the concentration of HCO_3^- in the deep aquifer is higher than in either the shallow aquifer water or the surface water. The decline of HCO_3^- could correlate closely with the TDS value. Figure 9c also shows two vertical lines: $\text{TDS} = 1$ and $\text{TDS} = 5$ g/L, to indicate the relationships between Na^+ , HCO_3^- , and TDS. The variation of the major hydrochemical concentrations in the direction of water runoff can be used as collateral evidence to explain the ongoing water recharging process in the Hopq Desert, i.e., from groundwater to soil water and then, to surface water.

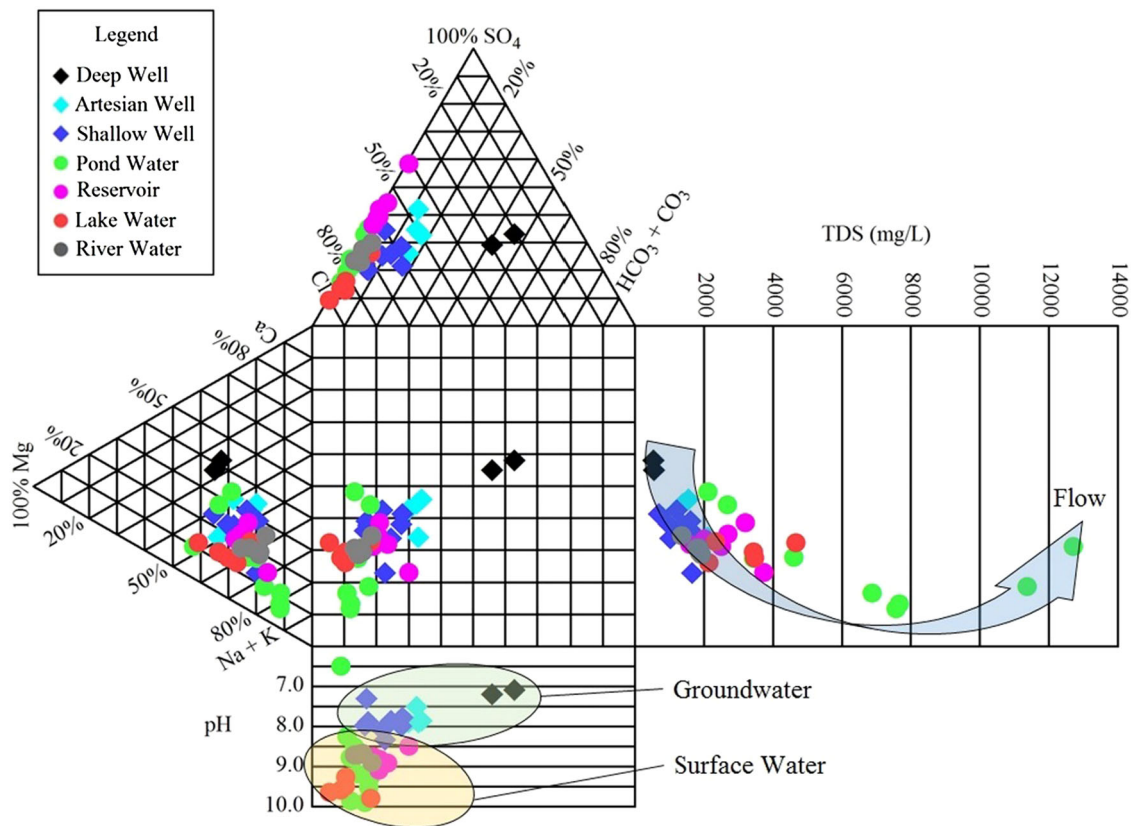


Fig. 8 Durov diagram showing major ion compositions of groundwater and surface water in the Hopq Desert

Discussion

Relationships of recharging between soil water and groundwater

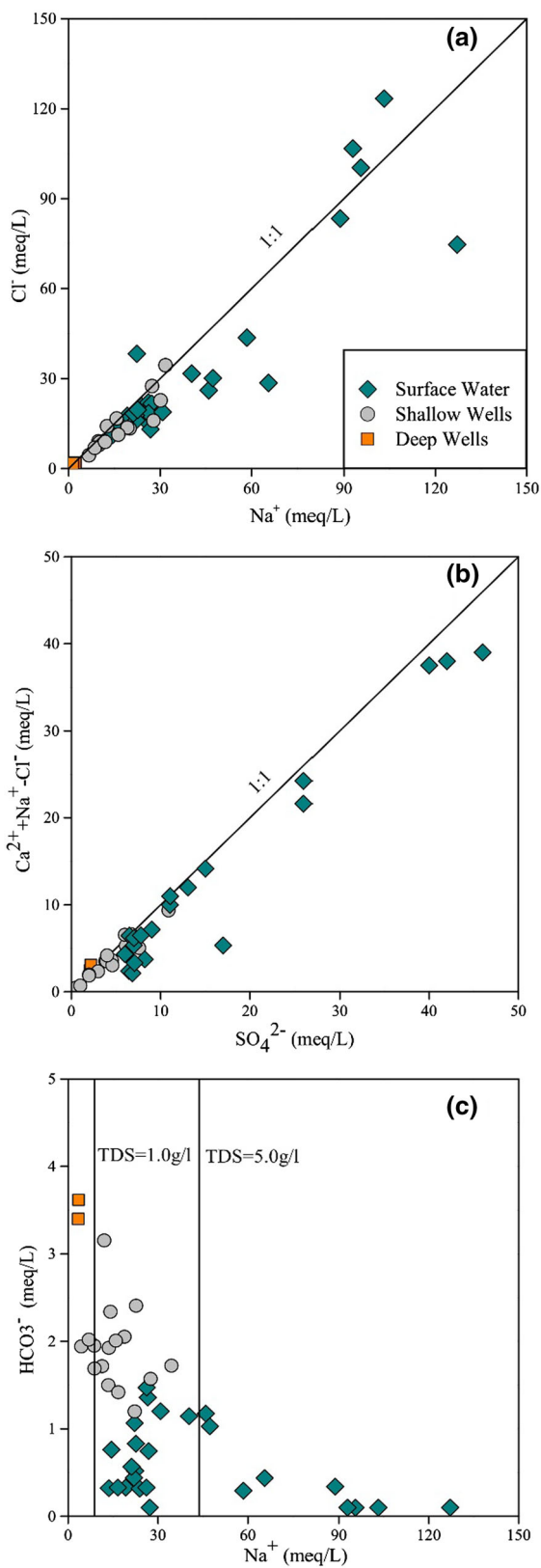
The soil profile analyses indicated that precipitation could not recharge the groundwater in the Hopq Desert. Although the porous sand layer is highly permeable, the moisture content profiles indicated that the vadose zone is in a state of water shortage because of the local episodic rainfall and intense evaporation. The limited amount of precipitation infiltrates only a short depth into the soil; however, the moisture within the topsoil can remain for only a short period because of the effects of the strong evaporation. Intense evaporation consumes the majority of pore water, which in turn, causes the moisture content to fall back to near zero. Thus, an ultra-dry sand layer such as this, with a depth varying from 20 to 30 cm, is found to cover the surface of the Hopq Desert (Fig. 7). It can protect the moisture in the deeper sand layers from evaporation loss [50]; however, it restricts the infiltration of precipitation because of the extremely low moisture content.

The analyses of the stable isotopes of hydrogen and oxygen in the different water samples indicated that δD and

$\delta^{18}O$ in the meteoric water are enriched in deuterium and oxygen 18, while the groundwater, soil water, and surface water are all depleted. The obvious difference between the values of δD and $\delta^{18}O$ implies that the groundwater, soil water, and surface water in the Hopq Desert could not be recharged by local precipitation. Based on the depleted stable isotopic signatures of the groundwater, further deductions regarding three essential prerequisites of the water source of the Hopq Desert groundwater could be inferred. First, the stable isotopic signatures should correspond to the Hopq Desert groundwater. Second, it should have a constant and ample magnitude of supply. Third, the underground transmission channels should be detectable.

Features of the external water recharging the Hopq Desert

The isotopic values of δD and $\delta^{18}O$ of the groundwater, surface water, soil water in the Hopq Desert, lake water in Qiangtang Basin, and precipitation in Lhasa [58] and northern China (major GNIP stations around the Hopq Desert, such as Baotou, Yinchuan, Xian, Lanzhou, and Taiyuan) are shown in Fig. 10. The δD and $\delta^{18}O$ relation points of Ordos precipitation (-7.64 , -51.43 ‰) are



◀**Fig. 9** Scatter plots of some of the major hydrochemical ions in the Hopq Desert (Units: meq/L). **a** Scatter plot of Na^+ versus Cl^- ; regression line is $y = 1.30x - 2.15$ ($n = 44$, $r^2 = 0.83$). **b** Scatter plot of $(\text{Ca}^{2+} + \text{Na}^+ - \text{Cl}^-)$ versus SO_4^{2-} ; regression line is $y = 0.87x - 0.48$ ($n = 44$, $r^2 = 0.76$). **c** Scatter plot of Na^+ versus HCO_3^- , indicating that in the process of water runoff from below, Na^+ ions become accumulated, HCO_3^- ions become depleted, and water quality deteriorates

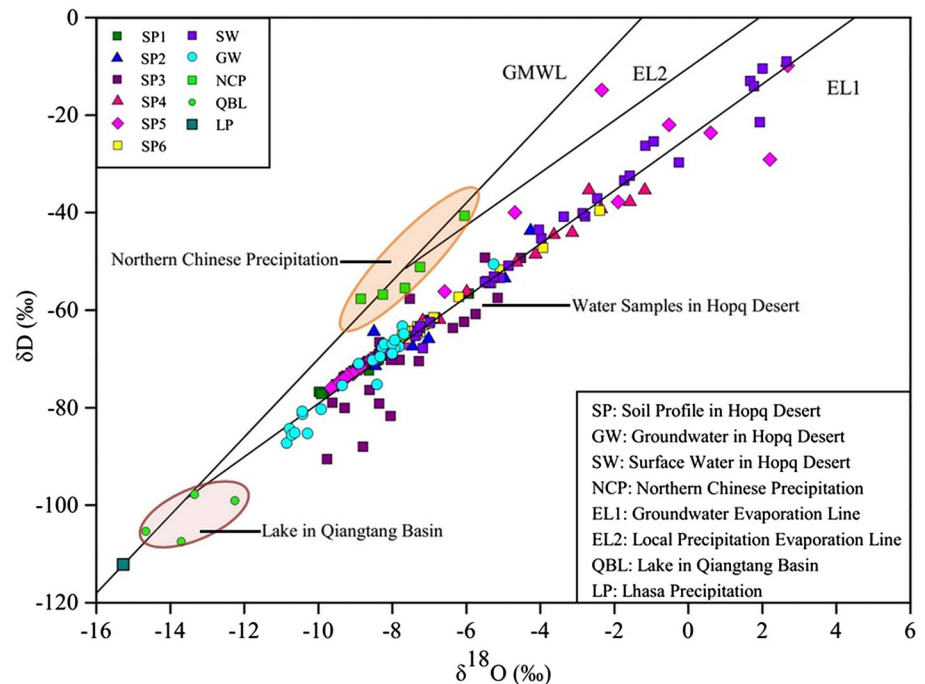
the water samples of the Hopq Desert. The intersection position of line EL1 and the global meteoric water line is lower than that of the precipitation of North China, but higher than that of the precipitation in the Lhasa area. The precipitation over the southwest to northeast part of the Tibetan Plateau is dominated by the Indian Ocean monsoon. Relatively, the precipitation in the Lhasa area is more depleted in deuterium and oxygen 18 than in the Qiangtang Basin (about 250 km north of Lhasa) [59]. Based on the deuterium and oxygen 18 signatures, the surface water in the Qiangtang Basin might satisfy the first of the three listed prerequisites and thus, it could possibly be the recharge water source of the Hopq Desert.

The Tibetan Plateau can be divided into an endorheic region and exorheic region. The endorheic region covers approx. $6.1 \times 10^5 \text{ km}^2$ and it has an annual average runoff of about 20.2 billion m^3 . The exorheic region covers an area of approx. $5.9 \times 10^5 \text{ km}^2$ and it has an annual average runoff of about 428 billion m^3 , i.e., about 21 times larger than that of the endorheic region, and from which many great rivers such as the Yangtze River, Yellow River, and Brahmaputra River originate. In order to comprehend the enormous difference in the runoff between the two regions, many investigations have been conducted. A balance analysis of the salt content in Nam Lake (northern Qiangtang Basin, the third largest salt lake in China) has revealed that the salt input from the supplying rivers is about 210 times larger than the salt content of the lake water. A water budget analysis established that water leakage from the Nam Lake is about 3.8–6.0 billion m^3/a [60]. Using field surveys, GIS, and satellite optical imagery methods, Chen et al. [17] confirmed that the rivers and lakes of the endorheic region of the Tibetan Plateau have massive water leakage.

Magnetotelluric sounding data have been used to determine the structure of the crust and upper mantle from central and northern parts of the Tibetan Plateau to the Qaidam Basin, Gansu Corridor, Ordos Basin, and Inner Mongolia Plateau. Widespread divisions of high conductivity and low wave transmission velocity were found to exist along the tectonic fault zones [61, 62]. Overlapping with the high conductivity and low wave transmission velocity layers, tectonic faults and structural rift belts were found to have a close relation with the seepage of rivers

enclosed within the range of North China precipitation. There are obvious differences in the values of deuterium and oxygen 18 between the North China precipitation and

Fig. 10 Isotopic values of δD versus $\delta^{18}O$ from groundwater, surface water, soil water in the Hopq Desert, lake water in the Qiangtang Basin, precipitation in Lhasa [58], and precipitation of North China (Baotou, Yinchuan, Xian, Lanzhou, and Taiyuan)



and lakes [63]. For example, the Jiali Fault runs west to east through the leakage area of the Nam Lake with resistivity of 10–16 Ω [64]. The temperature in the middle crust of the lithosphere is 375–600 $^{\circ}C$. If water-conducting structures exist, and if they had cooled down in the past, some geochemical evidence should be detectable in the outflow areas.

Regional magmatic activities have an intimate connection with the tectonic faults [65]. During our field survey, an east–west-aligned volcanic belt was discovered, centered on Tiemuerhada and extending for over 30 km (Fig. 11a). A volcanic masa ($40^{\circ}27.6'N$, $107^{\circ}55.2'E$; 1257 m a.s.l., i.e., relative height of 130 m) represents the highest point within the current study area. Unweathered igneous rocks and rhizoconcretions were found on the tops of some small monticules (Fig. 2g, h), similar to the rhizoconcretions discovered in the Badan Jaran Desert (400 km west of the Hopq Desert), which comprises a region of mega dunes and 144 lakes within an area of about 4.43×10^4 km² [66]. Previous studies have proven that rhizoconcretions are closely related to deep groundwater circulation [7, 50]. Widespread red sandstone strata (Fig. 2i) that constitute sedimentary rocks from the cementation of Quaternary aeolian sands contaminated with ferric oxide have also been discovered in the Hopq Desert [67]. The provenance of the magnesium in dolomite and the iron in red sandstone could be traced back to the magmatite in the middle crust, which has been proven to constitute the water transmission channel [68]. Ions such as Mg^{2+} and Fe^{2+} were extracted from the magmatic rocks

during the passage of the super-critical state water (SCW: 374.15 $^{\circ}C$, 22.1 Mpa) through the channel [69], following which the SCW upwelled into the sedimentary rocks, where Ca^{2+} and CO_3^{2-} were extracted from the limestone. When the temperature dropped, dolomitization occurred among the Ca^{2+} , Mg^{2+} , and CO_3^{2-} ions, while at the same time, Fe^{2+} ions reacted with oxygen to generate ferric oxide, which were all absorbed by the aeolian particles that comprised the red sandstone. Thus, trans-regional water recharges the Hopq Desert via the deep circulation channel, supporting the landscapes of the Hopq Desert [32].

Recharge, runoff, and discharge patterns of groundwater in the Hopq Desert

The coincidence of the distribution of the watersheds and bedrock fault zones (Fig. 11) was detected by the Chinese Geological Survey [33]. However, precipitation in the watershed region is about 200–300 mm/a, which almost equals that of the Hopq Desert. Figure 11 shows the main bedrock faults in Sishililiang and Gongqiriga, contours of groundwater level and precipitation in the current study area, and a model of how the external groundwater from the bedrock vents could recharge the Hopq Desert. As shown in Fig. 11b, the groundwater from the faults vents into the sedimentary strata, and the groundwater runoff is controlled by the permeability of the aquifer and the connections between the different aquifers [3], which are recharged from below. The schematic hydrological section indicates that the groundwater levels in most areas of the

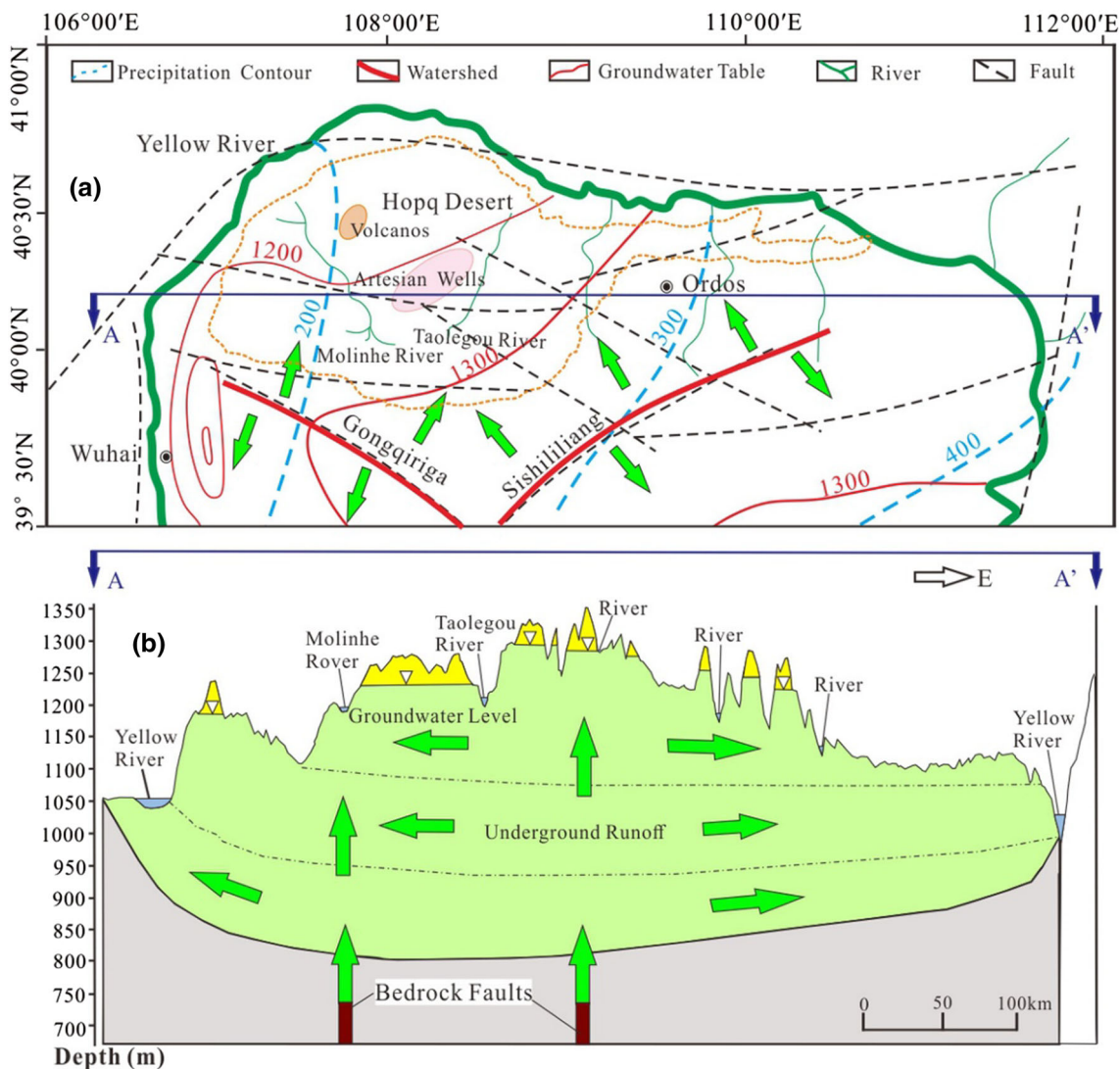


Fig. 11 Conceptual model of the recharge, runoff, and discharge relationship of the groundwater of the Hopq Desert. **a** Main bedrock faults, groundwater flows of Sishililiang and Gongqiriga, main rivers, and precipitation contours for the Hopq Desert. **b** Schematic

hydrological section in E–W direction indicating external water upwelling and discharging into the deep, medium, and shallow aquifers vertically and horizontally; different groundwater levels are also marked

Hopq Desert are higher than ground level, making the Hopq Desert an artesian basin. In low-lying areas, groundwater could overflow to the surface, forming rivers, lakes, and ponds. Thus, this model could explain the unusual phenomenon of better water quality in the deep aquifers than in the shallow aquifers of the Hopq Desert.

Conclusions

The vadose zone in the Hopq Desert is in a state of severe moisture shortage throughout most times of the year. The soil moisture content is far below the field water capacity, such that local precipitation can infiltrate only to a limited

depth within the topsoil. The pore water in the vadose zone is provided mainly by groundwater that flows upward, creating a unique model of vertical recharge of water from the saturated zone to the vadose zone in the Hopq Desert.

The major recharging source of the groundwater in the Hopq Desert is a type of trans-regional groundwater. The external groundwater discharges into the Hopq Desert, forming groundwater watersheds at Sishililiang and Gongqiriga. The groundwater flow field in the study area is dominated by the external groundwater and the water–rock interactions during underground runoff.

Analyses of the stable isotopes of hydrogen and oxygen, water budget, and geological structures indicated that the external water might originate as leakage water from the

Qiangtang Basin on the northern Tibetan Plateau. The evidence of volcanic basalt, dolomite, red sandstone, and rhizoconcretions within the study area suggests that super-critical water overflowed from discharge vents in bedrock fractures. This meant that the magnesium in the dolomite and ferric oxide in the red sandstone in the Hopq Desert were extracted from magmatic materials during the upward movement of the super-critical water, and that the water transmission channel had experienced a cooling process. In order to develop a rational plan for the exploitation and use of the groundwater resource of the Hopq Desert, our work suggests that future research should concentrate on the examination of the origin and migration of the external groundwater.

Acknowledgments This research was funded by the National Basic Research Program of China (2012CB417005), National Natural Science Foundation of China (51578212), and Fundamental Research Funds for the Central Universities (2014B17514, 2015B24614). The authors thank Tan Hongbing, Zhan Lucheng, and Huang Dewen for their support and considerate discussions. Special thanks to the anonymous reviewers for their critical reviews and supportive comments.

References

- Hou GC, Zhao MS, Wang YH et al (2006) Groundwater investigation in the Ordos Basin (in Chinese). China Geological Survey, Beijing
- Hou GC, Su XS, Lin XY et al (2007) Environmental isotopic composition of natural water in Ordos Cretaceous Groundwater Basin and its significance for hydrological cycle. *J Jilin Univ (Earth Science edn)* 37(2):255–260
- Hou GC, Liang YP, Su XS et al (2008) Groundwater systems and resources in the Ordos Basin, China. *Acta Geol Sin* 82(5):1061–1069
- Zhang MS, Hu FS, Yin LH (2008) Conceptual model of hydrogeology of the cretaceous groundwater basin of the Ordos Basin, China. *Geol Bull China* 27(3):1115–1122
- Yang YC, Shen ZL, Wen DG et al (2011) Formation and evolution of groundwater in the Ordos Cretaceous Basin: evidence from Chlorine and its isotope. *Acta Geol Sin* 85(4):586–595
- Chen JS, Yang GL, Wang T et al (2014) Soil water flow tracer test in northwest Ordos Basin, Inner Mongolia and discussion on recharge resources of artesian wells. *Acta Geol Sin* 35(3):365–374
- Chen JS, Chen XX, Wang T (2014) Isotopes tracer research of wet layer water sources in Alxa Desert. *Adv Water Sci* 2:196–206
- Su XS, Lin XY, Dong WH et al (2007) Application of inverse geochemical modeling in the correction of groundwater ^{14}C dating: advances and thoughts. *J Jilin Univ (Earth Science edn)* 37(2):271–277
- Yin LH, Hou GC, Tao ZP et al (2010) Origin and recharge estimates of groundwater in the ordos plateau, People's Republic of China. *Environ Earth Sci* 60(8):1731–1738
- Hou GC, Lin XY, Su XS, Wang XY et al (2006) Groundwater system in Ordos Cretaceous artisan Basin. *J Jilin Univ (Earth Science edn.)* 36(3):391–398
- Hou GC, Liang YP, Yin LH et al (2009) Groundwater systems and water resources potential in the Ordos Basin. *Hydrogeol Eng Geol* 36(1):18–23
- Li ZH, Zheng CB (2004) Evolution process of Paleo-karst and influence to reservoir: a case for Ordovician of Ordos Basin. *Nat Gas Geosci* 15(3):247–252
- Zhang JL, Cao ZL, Yu JM (2003) Exploration the origin of dolomite. *Mar Orig Petrol Geol* 6:109–115
- Chen JS, Wang T, Chen XX et al (2013) Discussion on the origin of groundwater in the Ordos Basin. *Geol Rev* 59(5):900–909
- Chen XX, Chen JS, Wang T (2014) Discussion about dating problems of northern groundwater in China. *Water Res Protect* 2:1–6
- Chen JS, Liu XY, Wang CY et al (2012) Isotopic constraints on the origin of groundwater in the Ordos Basin of northern China. *Environ Earth Sci* 66(2):505–517
- Chen JS, Wang QQ (2012) A discussion of groundwater recharge sources in arid areas of North China. *Water Res Protect* 3:5–12
- Allison GB, Gee GW, Tyler SW (1994) Vadose-zone techniques for estimating groundwater recharge in arid and semiarid regions. *Soil Sci Soc Am J* 58(1):6–14
- Carter RC, Morgulis ED, Dottridge J et al (1994) Groundwater modelling with limited data: a case study in a semi-arid dunefield of northeast Nigeria. *Q J Eng Geol Hydrogeol* 27:S85–S94
- Gaye CB, Edmunds WM (1996) Groundwater recharge estimation using chloride stable isotopes and tritium profiles in the sands of northwestern Senegal. *Environ Geol* 27(3):246–251
- Gee GW, Hillel D (1998) Groundwater recharge in arid regions: review and critique of estimation methods. *Hydrol Process* 2:256–266
- De Vries JJ, Simmers I (2002) Groundwater recharge: an overview of processes and challenges. *J Hydrol* 10:5–17
- Molla D, Stefan W, Tenalem A (2008) Major ion hydrochemistry and environmental isotope signatures as a tool in assessing groundwater occurrence and its dynamics in a fractured volcanic aquifer system located within a heavily urbanized catchment, central Ethiopia. *J Hydrol* 353:175–188
- Yuko A, Taro U, Nobuhito O (2002) Residence time and flow paths of water in steep unchanneled catchments, Tanakami, Japan. *J Hydrol* 261:173–192
- Aly AA (2015) Hydrochemical characteristics of Egypt western desert oases groundwater. *Arab J Geosci* 8(9):7551–7564
- Dogramaci S, Skrzypek G, Dodson W et al (2013) Stable isotope and hydrochemical evolution of groundwater in the semi-arid Hamersley Basin of sub-tropical northwest Australia. *J Hydrol* 475(26):281–293
- Song X, Wang P, Yu J et al (2011) Relationships between precipitation, soil water and groundwater at Chongling catchment with the typical vegetation cover in the Taihang mountainous region, China. *Environ Earth Sci* 62(4):787–796
- Paternoster M, Liotta M, Favara R (2008) Stable isotope ratios in meteoric recharge and groundwater at Mt. Vulture volcano, southern Italy. *J Hydrol* 348(1–2):87–97
- Rao BQ, Wang WB, Lan SB et al (2009) Development characteristics distribution of micro-organisms within 3-year-old artificial algal crusts in Hopq Desert. *Acta Hydrol Sin* 33(5):937–944
- Wei YF, Guo K (2008) Effect of precipitation pattern on recruitment of soil water in Kubuqi Desert, northwestern China. *J Plant Ecol* 32(6):1346–1355
- Huang T, Pang Z (2011) Estimating groundwater recharge following land-use change using chloride mass balance of soil profiles: a case study at Guyuan and Xifeng in the Loess Plateau of China. *Hydrogeol J* 19(1):177–186
- Chen JS, Liu Z, Liu XY (2013) Deep-circulation groundwater maintains continuous deposition of dusty particles in the Loess Plateau. *Acta Geol Sin* 87(2):278–287
- Li M, Gao J (2010) Basement faults and volcanic rock distributions in the Ordos Basin. *Sci China Earth Sci* 53(11):1625–1633

34. Allison GB, Hughes MW (1983) The use of natural tracers as indicators of soil-water movement in a temperate semi-arid region. *J Hydrol* 60:157–173
35. Shurabaji ARM, Philips FM, Campbell AR et al (1995) Application of a numerical model for simulation water flow, isotope transport and heat transfer in the unsaturated zone. *J Hydrol* 171:143–163
36. Neman BD (1996) Geochemical investigations of calcite fracture fills and mesa-top water dynamics on the Pajarito Plateau. Dissertation, New Mexico Institute of Mining and Technology
37. Socki RA, Karlsson HR, Gibson EK (1992) Extraction technique for the determination of oxygen-18 in water using pre-evacuated glass vials. *Anal Chem* 64(7):829–831
38. Coleman ML, Shepherd TJ, Durham JJ et al (1982) Reduction of water with zinc for hydrogen isotope analysis. *Anal Chem* 54(6):993–995
39. Gonfiantini R (1978) Standards for stable isotope measurements in natural compounds. *Nature* 271(5645):534–536
40. Coplen TB (1996) New guidelines for reporting stable hydrogen, carbon, and oxygen isotope-ratio data. *Geochim Cosmochim Acta* 60:3359–3360
41. Yang YC, Hou GC, Wen DG et al (2005) Hydrogen-oxygen isotope compositions of precipitation and seasonal effects on precipitation in Ordos Basin. *Acta Geosci Sin* 26:289–292
42. Liu JR, Song XF, Sun XM et al (2009) Isotopic composition of precipitation over Arid Northwestern China and its implications for the water vapor origin. *J Geogr Sci* 19(2):164–174
43. Craig H (1961) Isotopic variations in natural waters. *Science* 133:1702–1703
44. Zimmermann U, Ehhalt D, Muennich KO (1967) Soil–water movement and evapotranspiration: changes in the isotopic composition of the water. *Proc IAEA Symp Isotopes Hydrol* 1968:567–585
45. Gazis C, Feng X (2004) A stable isotope study of soil water: evidence for mixing and preferential flow paths. *Geoderma* 119(1–2):97–111
46. Dansgaard W (1964) Stable isotopes in precipitation. *Tellus A* 16(4):436–471
47. Zhao JB, Ke YU, Shao T et al (2011) A preliminary study on the water status in sand layers and its sources in the Tengger Desert. *Res Sci* 2:259–264
48. Feng Q, Cheng GD (1999) Moisture distribution and movement in sandy land of China. *Acta Pedol Sin* 36(02):225–236
49. Zhang WJ, Huang JT (2012) Distribution characters of precipitation in ordos basin. *J Arid Land Res Environ* 26(2):56–59
50. Chen JS, Li L, Wang JY et al (2004) Groundwater maintains dune landscape. *Nature* 432(7016):459–460
51. Nordstrom DK, Ball JW, Donahoe RJ, Whittemore D (1989) Groundwater chemistry and water-rock interactions at Stripa. *Geochim Cosmochim Acta* 53(8):1727–1740
52. O'Day PA, Carroll SA, Waychunas GA (1998) Rock-water interactions controlling zinc, cadmium, and lead concentrations in surface waters and sediments, US Tri-State Mining District. 1. Molecular Identification Using X-ray Absorption Spectroscopy. *Environ Sci Tech* 32(7):943–955
53. Rockware AqQA Software (2005) Version 1.1. <http://www.rockware.com>
54. Durov SA (1948) Natural waters and graphic representation of their composition. In *Dokl Akad Nauk SSSR* 59:87–90
55. Cary JW, Mayland HF (1972) Salt and water movement in unsaturated frozen soil. *Soil Sci Soc Am J* 36(4):549–555
56. Yang YC, Shen ZL, Wen DG et al (2008) Hydrochemical characteristics and sources of sulfate in groundwater of the ORDSO Cretaceous Groundwater Basin. *Acta Geosci Sin* 29(5):553–562
57. Crutzen PJ, Andreae MO (1990) Biomass burning in the tropics: impact on atmospheric chemistry and biogeochemical cycles. *Science* 250(4988):1669–1678
58. Zhang BZ, Zhang PX (1990) Distribution of hydrogen and oxygen isotopes in salt lakes of the Qinghai-Tibetan Plateau, China. *Chin J Geochem* 4(4):336–346
59. Liu JD, Zhao YC (1997) Discussion on the stable isotope time-space distribution law of china atmospheric precipitation. *Site Investig Sci Technol* 3:34–39
60. Zhou SQ, Kang S, Chen F et al (2013) Water balance observations reveal significant subsurface water seepage from Lake Nam Co, south-central Tibetan Plateau. *J Hydrol* 491:89–99
61. Xu CF (1996) The earthquake distribution and the resistivity structure in the Chinese mainland (i). *Acta Seismol Sin* 9(9):327–334
62. Jin S, Zhang LT, Jin YJ et al (2012) Crustal electrical structure along the Hezuo-Dajing profile across the northeastern margin of the Tibetan Plateau. *Chin J Geophys* 55(12):3979–3990
63. Jin S, Ye GF, Wei WB et al (2007) The electrical structure and fault feature of crust and mantle of western Tibetan Plateau: based on results of magnetotelluric survey along profile Zhada to Quanshuihu. *Earth Sci-J China Univ Geosci* 32(4):474–480
64. Wei WB, Jin S, Ye GF et al (2006) Conductivity structure of crust and upper mantle beneath the northern Tibetan Plateau: results of super-wide band magnetotelluric sounding. *Chin J Geophys* 49(4):1215–1225
65. Luo Z, Xiao X, Cao Y et al (2001) The Cenozoic mantle magmatism and motion of lithosphere on the north margin of the Tibetan plateau. *Sci China* 44(1 Suppl):10–17
66. Chen JS, Zhao X, Wang JY et al (2004) Meaning of the discovery of lacustrine tufa and root-shaped nodule in Badain Jaran Desert for the study on lake recharge. *Carsologica Sin* 23(4):277–282
67. Luo JL, Wei XS, Liu X (2010) Impact of provenance and diagenesis on sandstone reservoir quality of the Middle Permian in northern Ordos Basin, China. *Geochim Cosmochim Acta* 74(12):642
68. Chen JS, Jiang QN (2015) Research progress of ground water deep circulation. *Water Res Protect* 6:8–17
69. Manning CE (2013) Thermodynamic modeling of fluid-rock interaction at mid-crustal to upper-mantle conditions. *Rev Mineral Geochem* 76(1):135–164